SUPPORTING INFORMATION

Chinese Journal of Structural Chemistry

Graphene-Coated 1D $MoTe_2$ Nanorods as Anode for Enhancing Lithium-Ion Battery Performance

Shuwei Chai[1], Xiong Xiao[1], Yabei Li[1] and Changhua An[1]*

[1]*Tianjin Key Laboratory of Organic Solar Cells and Photochemical Conversion, School of Chemistry and Chemical Engineering, and Tianjin Key Laboratory of Advanced Functional Porous Materials, Institute for New Energy Materials & Low-Carbon Technologies, Tianjin University of Technology, Tianjin 300384, China*

**Corresponding author. Email: anchua@ustc.edu*

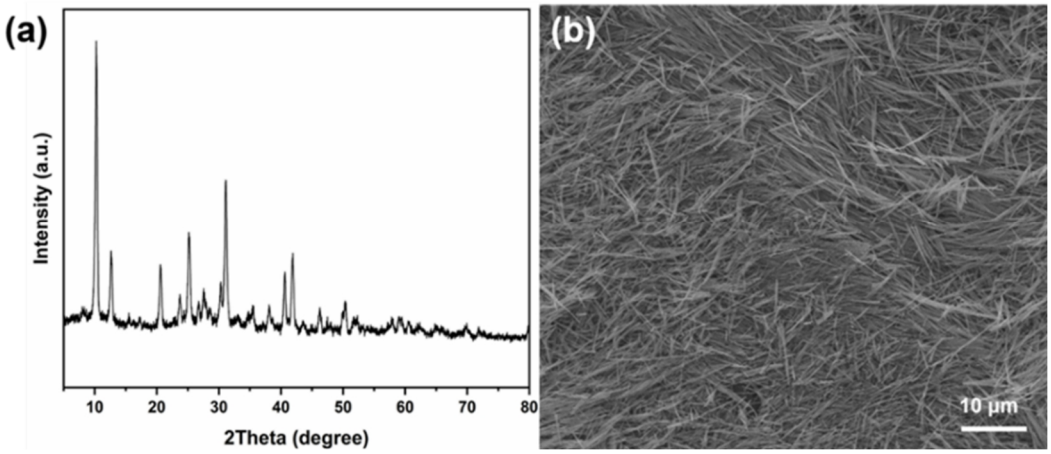

Figure S1. (a) XRD pattern of $Mo_3O_{10}(C_2H_{10}N_2)$ and (b) SEM image of $Mo_3O_{10}(C_2H_{10}N_2)$ nanowires.

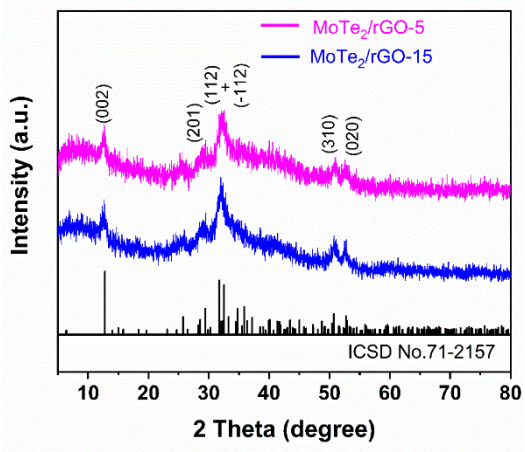

Figure S2. XRD patterns of $MoTe_2$/rGO-5 and $MoTe_2$/rGO-15 nanocomposites.

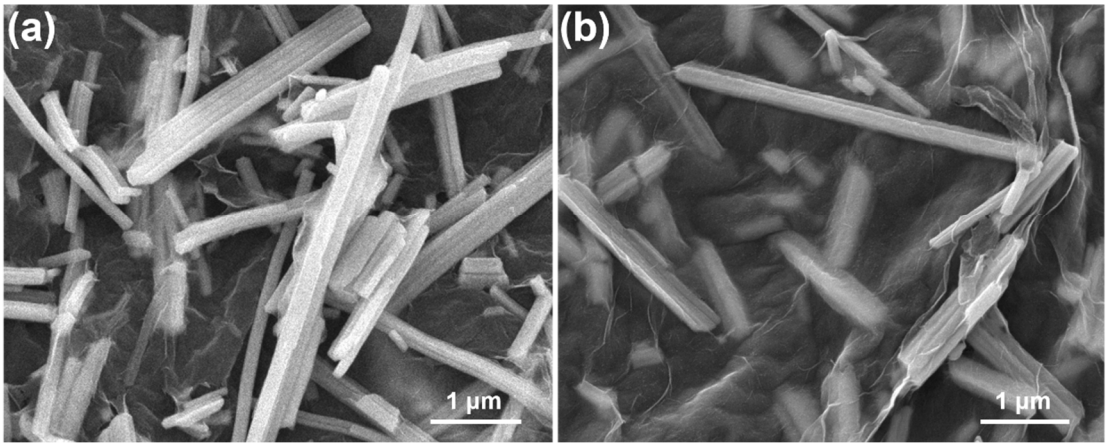

Figure S3. SEM images of (a) $MoTe_2$/rGO-5 and (b) $MoTe_2$/rGO-15 nanocomposites.

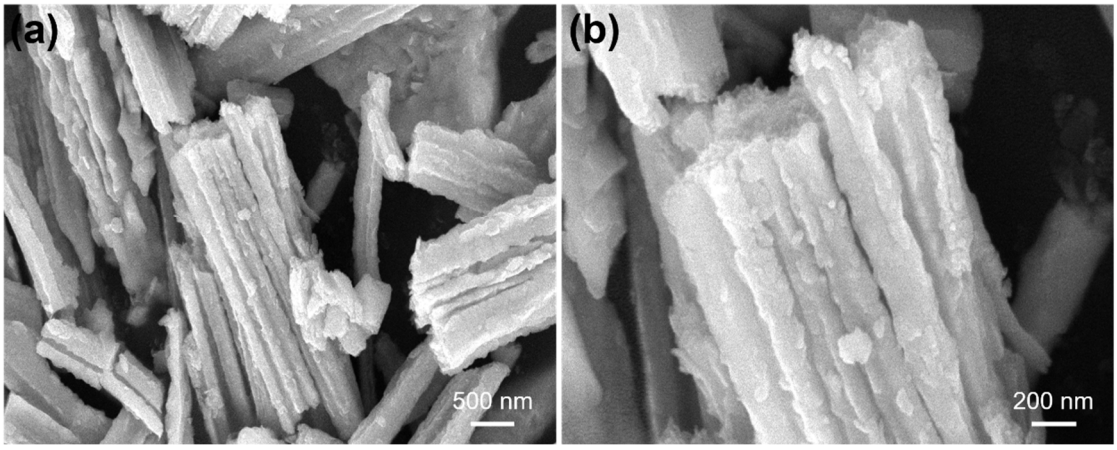

Figure S4. Low- (a) and high-magnification (b) SEM images of bare $MoTe_2$ nanorods.

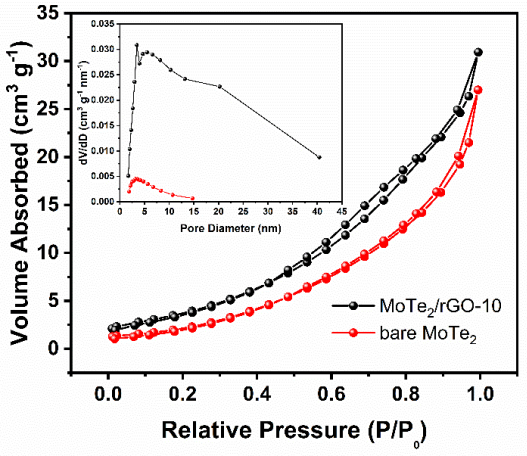

Figure S5. Nitrogen adsorption and desorption isotherms of bare $MoTe_2$ and $MoTe_2$/rGO-10 nanocomposite.

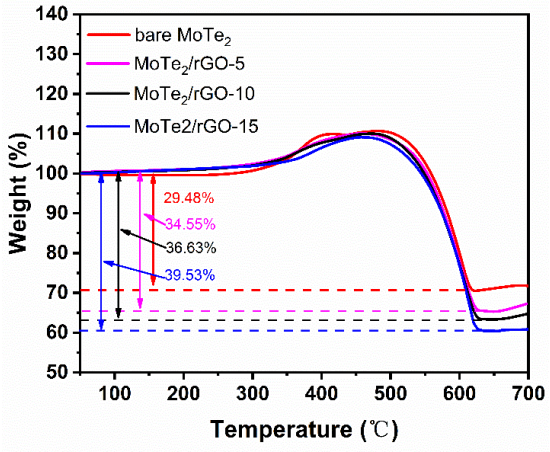

Figure S6. TGA curves of bare $MoTe_2$, $MoTe_2$/rGO-5, $MoTe_2$/rGO-10, and $MoTe_2$/rGO-10 nanocomposites.

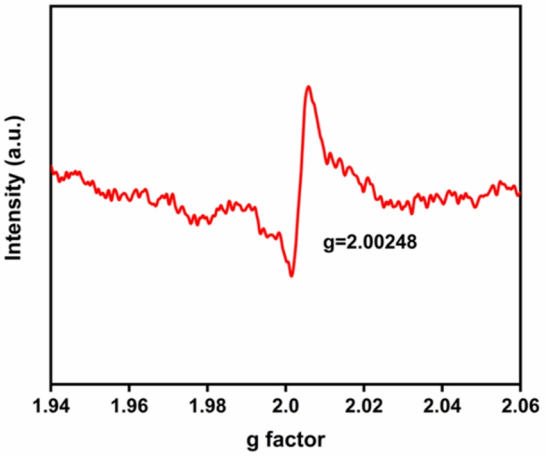

Figure S7. EPR spectrum of $MoTe_2$/rGO-10 nanocomposite.

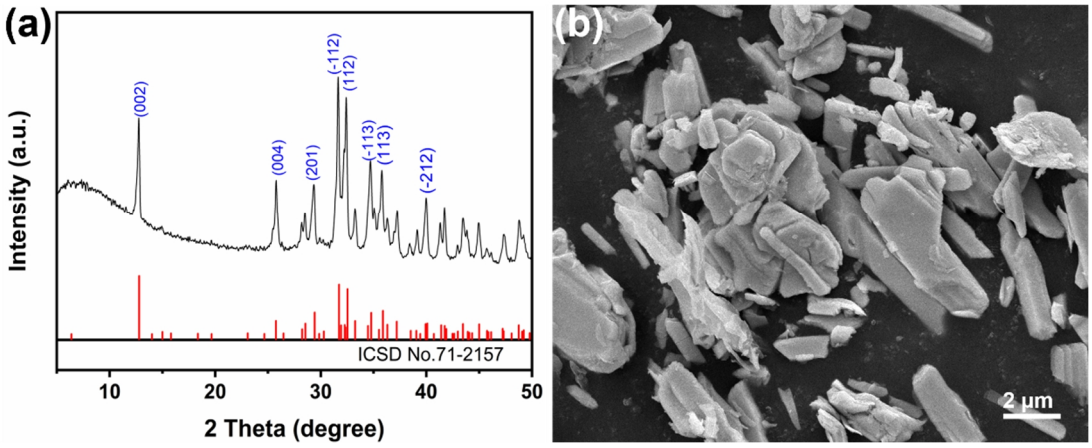

Figure S8. (a) XRD pattern and (b) SEM image of bulk $MoTe_2$.

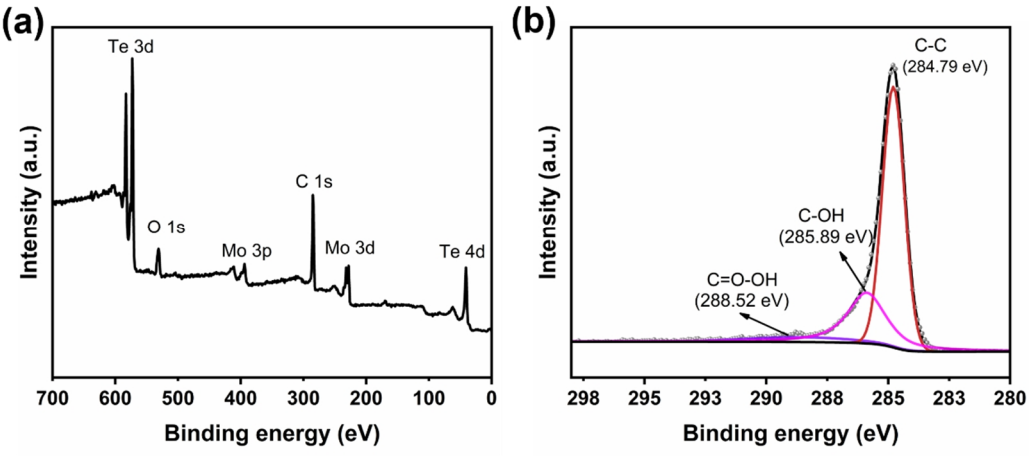

Figure S9. (a) Survey XPS, and (b) high resolution C 1s spectrum of $MoTe_2$/rGO-10 nanocomposite.

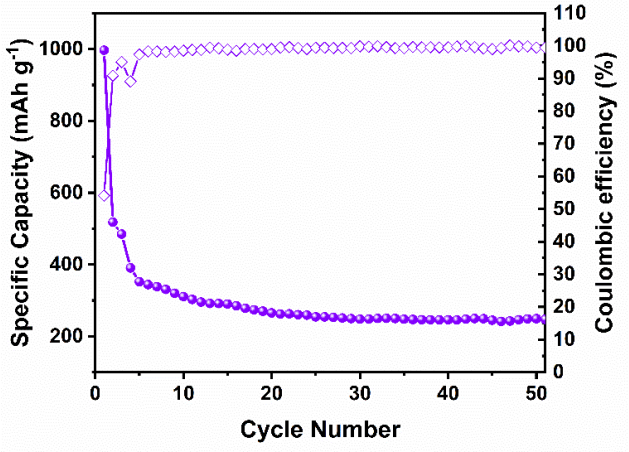

Figure S10. Cycling performance of the bare rGO coating at 0.2 A g^{-1}.

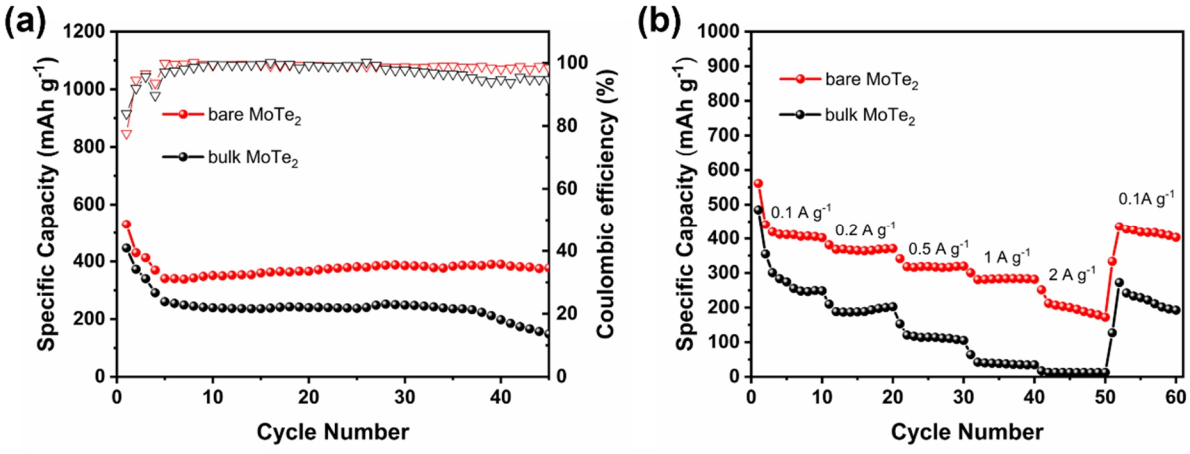

Figure S11. (a) Cycling performance at 0.2 A g^{-1} and (b) rate capability of bare $MoTe_2$ and bulk $MoTe_2$.

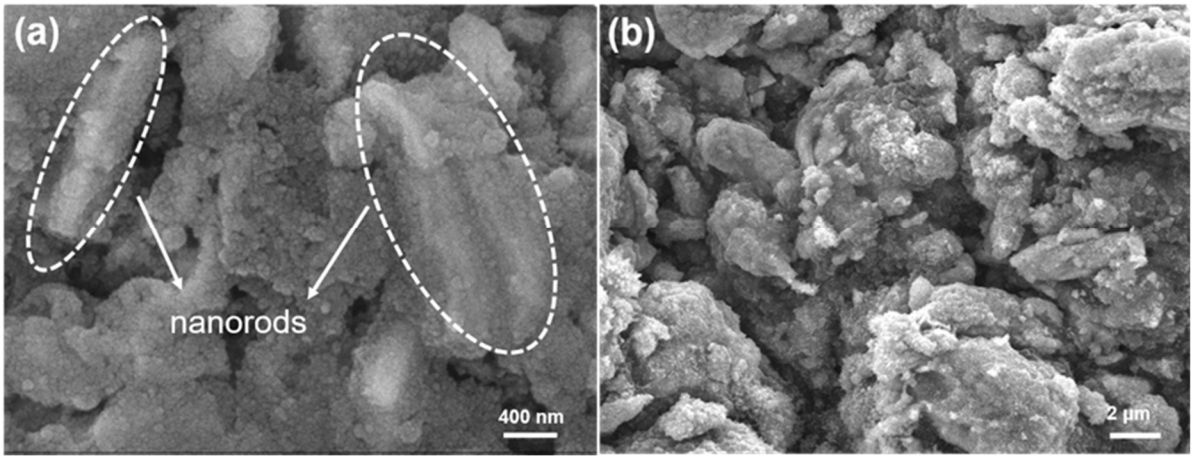

Figure S12. SEM images of $MoTe_2$/rGO-10 nanocomposite (a), and bulk $MoTe_2$ (b) electrode after 100 cycles at 0.2 A g^{-1}.

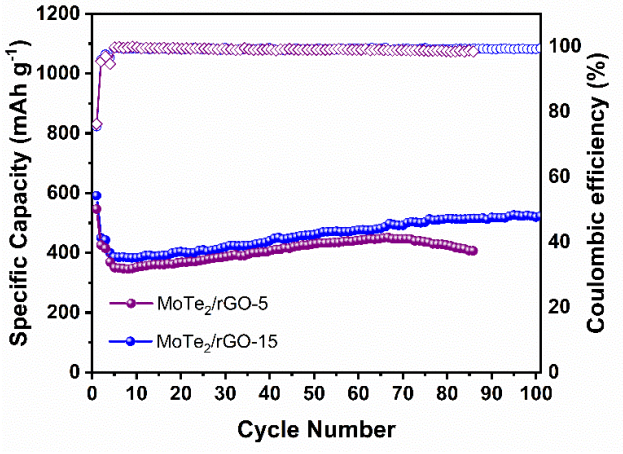

Figure S13. Cycling performance of the bare $MoTe_2$ nanorods and $MoTe_2$/rGO-10 composite at 0.2 A g^{-1}.

The Li^+ diffusion coefficient (D) was yielded by galvanostatic intermittent titration technique (GITT) based on the following Eq. S1:

$$D = \frac{4}{\pi\tau}\left(\frac{m_B V_m}{M_B S}\right)^2 \left(\frac{\Delta E_s}{\Delta E_t}\right)^2 \qquad \text{Eq. S1}$$

where τ represents the relaxation time (s), m_B is the mass of active material (g), V_m represents the molar volume of active material, M_B is the molar mass of active material (g/mol), ΔE_s represents the steady-state voltage change (V) by the current pulse, and ΔE_t is the voltage change (V) during the constant current pulse after eliminating the iR drop, respectively.

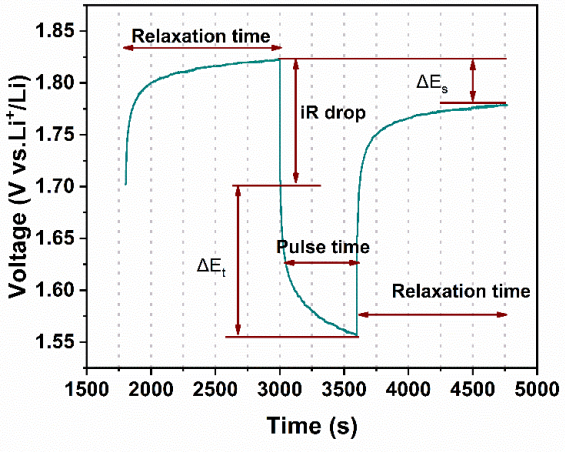

Figure S14. Voltage vs. time profile of $MoTe_2$/rGO-10 electrode for a single GITT titration.

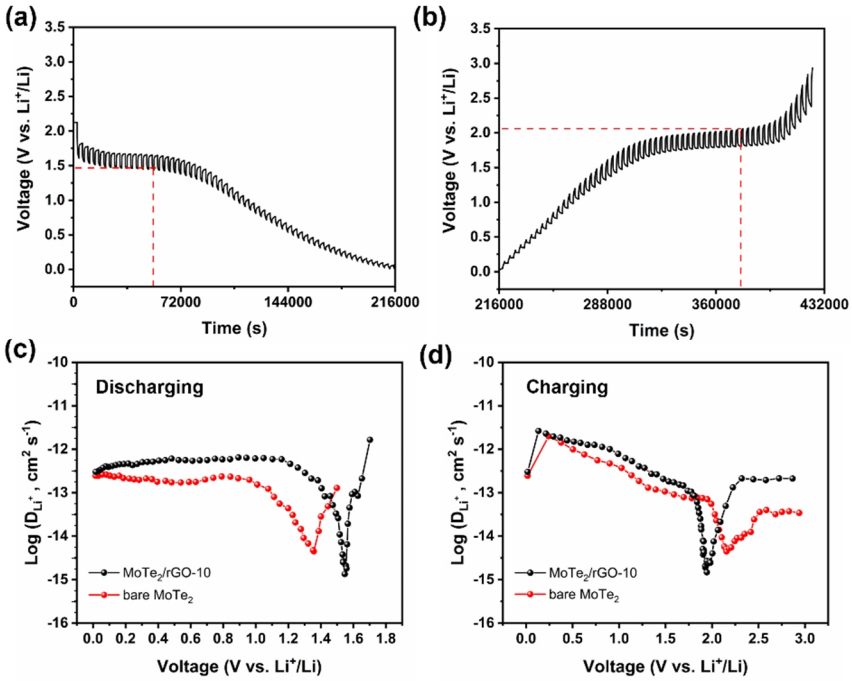

Figure S15. GITT profiles of $MoTe_2$/rGO-10 electrode at discharge (a) and charge state (b); Li^+ diffusion coefficient at (c) discharge and (d) charge process.

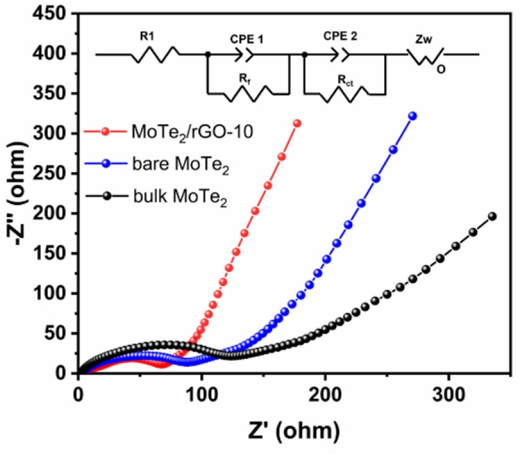

Figure S16. Nyquist plots and equivalent circuit for the EIS analysis of the bare $MoTe_2$, bulk $MoTe_2$ and $MoTe_2$/rGO-10 nanocomposite.

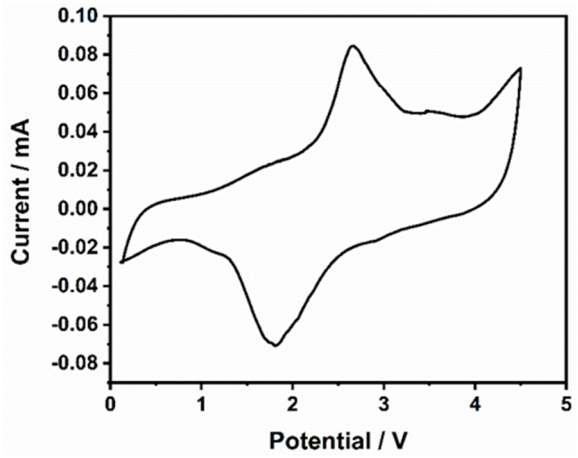

Figure S17. CV curve of $MoTe_2$/rGO-10//LCO full cell at a scan rate 0.1 mV s^{-1} in the potential window of 0.1-4.5 V.

Table S1. Comparison of the Conventional Anode Materials and Our $MoTe_2$/rGO Nanocomposite Anode Configuration

Anode material	Current rate (A g^{-1})	Discharging capacity (mA h g^{-1})	Cycling retention	Reference
pristine $MoTe_2$	1	291	260	[1]
$MoTe_2$/FLG	0.1	150	596.5	[2]
1D-$MoTe_2$ film	0.05	770	1st	[3]
$MoSe_2$/C nanorods	0.2	200	755	[4]
$MoSe_2$/C	0.2	618	300	[5]
MoO_2-carbon nanowires	0.2	500	20	[6]
MoO_2-loaded porous carbon hollow sphere	0.05	640	80	[7]
MoS_2@$Ti_3C_2T_x$	1	132	275	[8]
p-Ti_3C_2/MoS_2	0.5	230	50	[9]
$MoTe_2$/rGO	**0.2/0.5**	**637/320**	**100/200**	**Our work**

n REFERENCES

(1) Panda, M. R.; Gangwar, R.; Muthuraj, D.; Sau, S.; Pandey, D.; Banerjee, A.; Chakrabarti, A.; Sagdeo, A.; Weyland, M.; Majumder, M.; Ban, Q. L.; Mitra, S. High performance lithium-ion batteries using layered 2H-$MoTe_2$ as anode. *Small* **2020**, 16, 2002669.

(2) Ma, N.; Jiang, X. Y.; Zhang, L.; Wang, X. S.; Cao, Y. L.; Zhang, X. Z. Novel 2D layered molybdenum ditelluride encapsulated in few-layer graphene as high-performance anode for lithium-ion batteries. *Small* **2018**, 14, 1703680.

(3) Kim, E. K.; Yoon, S. J.; Bui, H. T.; Patil, S. A.; Bathula, C.; Shrestha, N. K.; Im, H.; Han, S. H. Epitaxial electrodeposition of single crystal $MoTe_2$ nanorods and Li^+ storage feasibility. *J. Electroanal. Chem.* **2020**, 878, 114672.

(4) Qiong, S.; Cao, X. X.; Kong, X. Z.; Wang, Y. P.; Peng, C.; Chen, J.; Yin, B.; Shi, J. R.; Liang, S. Q.; Pan, A. Q. Carbon-encapsulated $Mose_2$/C nanorods derived from organic-inorganic hybrid enabling superior lithium/sodium storage performances. *Electrochim. Acta* **2018**, 292, 339-346.

(5) Qin, F. R.; Hua, H. X.; Jiang, Y. J.; Zhang, K.; Fang, Z.; Lai, Y. Q.; Li, J. Mesoporous $MoSe_2$/C composite as anode material for sodium/lithium ion batteries. *J. Electroanal. Chem.* **2018**, 823, 67-72.

(6) Gao, Q. S.; Yang, L. C.; Lu, X. C.; Mao, J. J.; Zhang, Y. H.; Wu, Y. P.; Tang, Y. Synthesis, characterization and lithium-storage performance of MoO_2/carbon hybrid nanowires. *J. Mater. Chem.* **2010**, 20, 2807.

(7) Gao, H.; Liu, C. L.; Liu, Y.; Liu, Z. H.; Dong, W. S. MoO_2-loaded porous carbon hollow spheres as anode materials for lithium-ion batteries. *Mater. Chem. Phys.* **2014**, 147, 218.

(8) Shen, C. L.; Wang, L. B.; Zhou, A. G.; Zhang, H.; Chen, Z. H.; Hu, Q. K.; Qin, G. MoS_2-Decorated Ti_3C_2 MXene nanosheet as anode material in lithium-ion batteries. *J. Electrochem. Soc.* **2017**, 164, A2654.

(9) Zheng, M.; Guo, R. S.; Liu, Z. C.; Wang, B. Y.; Meng, L. C.; Li, F. Y.; Li, T. T.; Luo, Y. N. MoS_2 intercalated p-Ti_3C_2 anode materials with sandwich-like three dimensional conductive networks for lithium-ion batteries. *J. Alloy Compd*. **2018**, 735, 1262.